Reac Kinet Mech Cat (2016) 117:815–827
DOI 10.1007/s11144-015-0949-6

Decolorization kinetics of the direct red 23 diazo dye from zinc/cobalt mixed oxide semiconductor using oxalate as a precursor

Vanildo Souza Leão Neto[1] · Thiago Orcelli[1] · Marcelo Rodrigues da Silva[2] · Fauze Jacó Anaissi[3] · Keiko Takashima[1]

Received: 12 August 2015 / Accepted: 1 November 2015 / Published online: 13 November 2015

Abstract In this paper, we report the oxidation kinetics of the Direct Red 23 diazo dye through the UV irradiation of an aqueous suspension of zinc/cobalt mixed oxide semiconductor at 30 °C. The zinc and cobalt mixed oxide was prepared by the thermal decomposition of their oxalates, containing 5, 10, and 20 % (w/v) cobalt and calcined at 400 °C for 12 h. The characterization of these oxides was performed by X-ray diffraction, thermal and thermo-gravimetric analysis, X-ray dispersive energy spectrometry, scanning electron microscopy, diffuse reflectance spectroscopy, and textural analysis to understand the physical and chemical behavior of these materials. The suspension, formed by synthesized oxide and the Direct Red 23 diazo dye, was kept for 60 min in the dark and, subsequently irradiated during 210 min. The decolorization rate constant, k_{obs}, was determined under pseudo-first order conditions, maintaining the semiconductor concentration much larger than the diazo dye concentration, using the maximum Direct Red 23 absorbance at 503 nm, and plotting the natural logarithm as a function of irradiation time at 30 °C. All the synthesized mixed oxides displayed higher photocatalytic activity in comparison to commercial zinc oxide. From these, the oxide containing 5 % cobalt showed the highest photocatalytic activity, resulting in a rate constant for the Direct Red 23 diazo dye equivalent to 14.0×10^{-3} min^{-1} or 93 % decolorization at 30 °C.

Keywords Diazo dye oxidation · Heterogeneous photocatalysis · Photocatalytic activity · Oxide characterization

✉ Keiko Takashima
keiko.takashima@gmail.com

[1] Laboratório de Processos de Oxidação Avançados, Department of Chemistry, Universidade Estadual de Londrina, Caixa Postal 10011, Londrina, Paraná 86057-970, Brazil

[2] Faculdade de Engenharia, Universidade Estadual Paulista, São Paulo, Bauru, Brazil

[3] Department of Chemistry, Universidade Estadual do Centro-Oeste, Guarapuava, Paraná, Brazil

Introduction

Several sectors of industrialized countries face environmental problems related to water contamination, which deserve special attention, because of the high loading of organic and inorganic pollutants. Within this segment, textile dyes have caused significant pollution because of the discarding of the colored effluent into the environment is a source of aesthetic pollution, besides the adverse effects on aquatic life [1]. Considering that environmental pollution is a major problem faced by contemporary society, many studies have been focused on the preservation of aquatic and atmospheric environments using advanced oxidation processes as a tool. Most of the dyes used in textile industries are of the azo type, characterized by one or more azo groups (N=N), bonded to the sp^2 carbon atoms, as benzene or naphthalene rings. Although these dyes are present in approximately 20 % of textile industry effluents, research about these compounds is very important for several reasons [2]. Among these, there are removal difficulties by the traditional processes and due to mutagenic and carcinogenic effects. So, the Direct Red 23 diazo dye, DR23 ($C_{35}H_{27}N_7S_2O_{10}Na_2$, C.I. 29160) (Fig. 1) is a molecule model to study the removal dye of the wastewater.

Advanced oxidation processes (AOPs) have attracted great interest for the oxidation of organic matter because under appropriate conditions, species are removed and converted completely into CO_2, H_2O, and harmless minerals. AOPs are based on the hydroxyl radical (HO·) generation. This radical is characterized by non-specificity, high oxidizing power ($E_o = 2.8$ V), and short lifetime [3, 4]. Oxidation and reduction processes occur on the surface or in the vicinity of the photo-excited semiconductor particle. Among the processes that produce hydroxyl radical, heterogeneous photocatalysis has been shown as one of the promising method in the destruction of a variety of organic compounds over the past decades. It is based on the irradiation of an n-type semiconductor as TiO_2, ZnO, etc., whose photon energy (hν) must be greater or equal to the band gap energy (E_{bg}), mineralizing organic compounds and simultaneously reducing dissolved metals or other species [5–7]. Consequently, the semiconductor oxides have been widely investigated in the fighting of environmental pollution by heterogeneous photocatalysis. Transition metal oxides draw attention for use as photocatalysts because they combine the d electrons, nanometric size, and large surface area, in addition to the lower cost alternative [8].

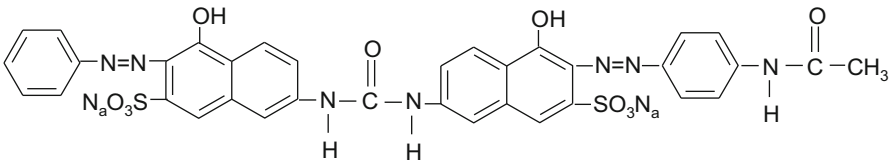

Fig. 1 Structural formula of Direct Red 23 (DR23) acid 3-[[4-(acetylamino)phenyl]azo]-4-hydroxy-7-[[[[5-hydroxy-6-(phenylazo)-7-sulfo-2-naphtalenyl]-amino]carbonil]amino]-2-naftalenosulfonate of sodium (IUPAC nomenclature)

Zinc oxide has been widely studied due to the above mentioned properties, which make it a large technological potential material. ZnO presents the structure of wurtzite type, band gap of 3.37 eV, excitons binding energy of 60 meV, high electron mobility and good transparency [9]. Among other technological applications used are gas sensors [10], solar cells [11], biosensors [12], etc. ZnO is regarded as a non-stoichiometric compound, due to the Zn^{2+} excess in the interstitial lattice positions. Thus, in order to maintain electroneutrality, additional electrons are found in the oxide lattice, acquiring the n-type semiconductor behavior [13–15]. Since it is very important to find alternatives to pollutant decontamination, several studies have been conducted in order to increase the photocatalytic efficiency of the semiconductor oxides. Among these, doping oxides have been investigated to generate a p-n junction in the mixed oxides. Hence, the p-type semiconductor as Co_3O_4 is also a non-stoichiometric compound with O^{2-} excess in the lattice with balanced positive charges in the interstices. This means that when a p-type semiconductor is placed in contact with an n-type, a double layer of charges is formed in the junction. The p-n junction is based on non-recombination of the electron–hole pair, which prevents the electron passage to the p-region and the holes for n-region. This generates a different electrostatic potential on both sides and produces a lack of carriers, called depletion region in the interface [16, 17]. For instance, Wang et al. synthesized p-CuO/n-$BiVO_4$ mixed oxide and applied to the Rhodamine B degradation [18]. Furthermore, da Silva et al. synthesized a mixed oxide containing n-$BiVO_4$ and p-NiO in order to degrade the methylene blue [19]. In both cases, there was an enhancement of the photocatalytic activity, attributed to the formation of the p-n junction in relation to the pure semiconductor. Moreover, the p-n junction formation using n-ZnO attracted attention to improve the photocatalytic activity of this important oxide [20, 21].

Among the p-type semiconductors, cobalt oxide has been widely used in reactions for the production of H_2 [22], in alkaline batteries [23], organic pollutants degradation through the catalytic and electrochemical reactions [24]. Cobalt oxide has five species [CoO_2, Co_2O_3, CoO(OH), Co_3O_4, and CoO] with a wide range of applications in various industrial sectors. The Co_3O_4 spinel has a band gap energy ranging from 1.4 to 1.8 eV and is stable up to 800 °C [25]. Owing to these properties, it is expected that cobalt oxide addition in zinc oxide could promote the p-n junction formation and also, to enhance the photocatalytic activity.

This study aimed at determining the photocatalytic activity of the prepared mixed oxide and compared it to that of the commercial ZnO by the means of the decolorization rate constant of the Direct Red 23 diazo dye at 30 °C. The mixed oxide was prepared by the thermal decomposition of the zinc and cobalt mixed oxalate containing 5, 10, and 20 % cobalt and calcined at 400 °C during 12 h. These materials were characterized by several structural and morphological techniques such as scanning electron microscopy, X-ray diffraction (XRD), thermogravimetry and differential thermal analysis, textural analysis, UV/Vis spectroscopy coupled to diffuse reflectance sphere, among others.

Experimental

Preparation of the zinc and cobalt mixed oxide

The mixed oxide of zinc and cobalt was prepared according to Muruganandham et al. [26]. The mixed oxide containing 5 % cobalt was prepared using equal volumes of 0.40 mol L^{-1} zinc nitrate [$Zn(NO_3)_2{\cdot}6H_2O$, Synth 99.5 %], 2.0 × 10^{-2} mol L^{-1} cobalt nitrate [$Co(NO_3)_2{\cdot}6H_2O$, Vetec 98.8 %], and 0.60 mol L^{-1} anhydrous oxalic acid ($H_2C_2O_4$, Belga 99 %) in deionized water (Milli-Q Plus), which were boiled separately. At this temperature, solutions of zinc nitrate and cobalt nitrate were immediately added to the oxalic acid and the heating stopped. The resulting mixture was kept under agitation (600 rpm—301 Microquímica AMA) at room temperature. The formed precipitate was filtered under vacuum (Schleicher Schuell 0.47 ± 0.5 mm diameter, pore 0.2 μm) and washed several times with distilled water, maintained overnight at room temperature, and dried at 100 °C (BioPar S150SD) for 3 h. About 2.0 g of the compound was introduced into the muffle (Marconi MA385) and heated from 5 to 10 °C min^{-1} at a calcination temperature of 400 °C for 12 h. The procedure was repeated for 10 and 20 % (w/v) cobalt in the mixed oxide.

Characterization

The thermal decomposition of zinc and cobalt oxalate was evaluated by thermogravimetry (TG) and differential thermal analysis (DTA) at a heating rate of 10 °C min^{-1} from 30 to 1200 °C in air atmosphere using alumina as reference material (Seiko 6300). XRD data was collected in a Rigaku D/Max–2100PC instrument at room temperature, using Cu K_α radiation (1.5418 Å) radiation, coupled to a nickel filter, in order to reduce the unfavorable Cu K_β radiation. The applied tension was 40 kV and the current was 30 mA. The scanning range was from 10 to 80° with regular step of $1°s^{-1}$. Current and voltage were 20 mA and 40 kV, respectively. The band gap energy of the oxides was determined using the diffuse reflectance spectra (Shimadzu UV-3101PC) by Kubelka–Munk and Tauc methods. The textural analysis was performed, preheating the sample at 300 °C under vacuum for 3 h to measure the surface area, pore volume and pore radius (Quantachrome NovaWin version 10:01). The morphology of the oxides was studied by scanning electron microscopy (Philips FEI Quanta 200). The distribution and the surface composition were determined by X-ray dispersive energy spectroscopy (EDX) using the same microscope. The elemental composition was determined by X-ray fluorescence (Shimadzu EDX-720).

Photocatalysis

The photocatalytic activity was determined inside a wooden box (50 × 50 × 50 cm^3) with internal walls covered with aluminum foil and closed frontally with black curtain in a double wall borosilicate glass reactor (200 mL) with water

circulation at 30.0 ± 0.1 °C (Microquímica MBQTC99-20). The suspension formed by 0.7 g L^{-1} oxide in 150 mL of 7.5 × 10^{-5} mol L^{-1} DR23 diazo dye (Chimical—30 % dye content) was stirred at 600 rpm (Fisatom 752) in the dark for 60 min and irradiated by a mercury vapor lamp without bulb (Phillips HPL-N 125W with wavelengths from ~350 to 450 nm) positioned horizontally at 22 cm of the suspension surface during 210 min. Aliquots of 1.5 mL were collected at predetermined times and UV–Vis spectra (200–700 nm) recorded (Hitachi U3000). The decolorization rate constant, k_{obs}, was determined under pseudo-first order conditions , maintaining the semiconductor concentration much larger than the diazo dye, using the maximum of Direct Red 23 absorbance at 503 nm, with a molar absorptivity of 2.17 × 10^4 L cm^{-1} mol^{-1}, and plotting the natural logarithm as a function of irradiation time at 30 °C. The decolorization percentage of DR23 was determined spectrophotometrically by measuring dye absorbance at λ_{max} 503 nm. The decolorization efficiency (%) was calculated as given in Eq. 1, where A_0 is the initial dye absorbance, and A is the absorbance after irradiation.

$$Efficiency\ (\%) = \frac{A_0 - A}{A_0} \times 100 \quad (1)$$

Results and discussion

Fig. 2 shows the TG and DTA decomposition of 5 % cobalt in zinc and cobalt mixed oxalate. The mass losses occurred at the same temperatures for 10 and 20 % cobalt. The initial loss at 175 °C is an endothermic process that corresponds to the dehydration as shown in Eq. 2 [27].

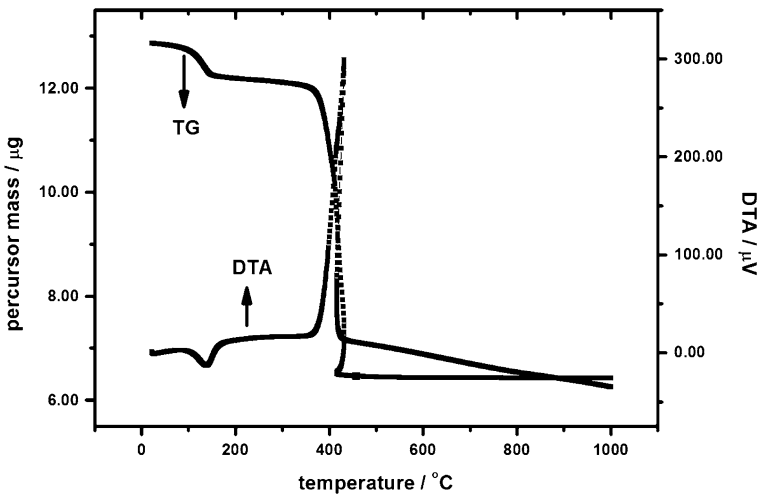

Fig. 2 TG/DTA of zinc and cobalt mixed oxalate containing 5 % Co with 10 °C min^{-1} in air atmosphere

$$ZnC_2O_4{\cdot}CoC_2O_4{\cdot}(3.7)H_2O \rightarrow ZnC_2O_4{\cdot}CoC_2O_4 + (3.7)H_2O \quad (2)$$

The second loss at 400 °C took place exothermically and corresponds to the oxidation of the mixed oxalate ($ZnC_2O_4{\cdot}CoC_2O_4$) in mixed oxide ($ZnO{\cdot}Co_3O_4$), CO_2, and CO, as shown in Eq. 3.

$$3ZnC_2O_4{\cdot}3CoC_2O_4 \rightarrow 3ZnO{\cdot}3Co_3O_4 + 5CO_2 + 7CO \quad (3)$$

The Co_3O_4 spinel is stable up to 800 °C, whose crystal structure releases oxygen above 900 °C, forming ZnO·CoO that corresponds to the third loss at 904 °C shown in Eq. 4 [28].

$$3ZnO{\cdot}3Co_3O_4 \rightarrow 3ZnO{\cdot}3CoO + O_2 \quad (4)$$

The thermal decomposition of zinc and cobalt oxalate in other proportions occurred also in three stages in air atmosphere as shown in TG/DTA curves in Fig. 2. Even though the oxide is stable from 400 to 800 °C, the samples were calcined at 400 °C, due to the existing defects in the structure, which are dependent on the calcination temperature, that is, the lower sample crystallization, the lower e^-/h^+ pair recombination, and consequently, the higher catalytic activity.

Fig. 3 displays the XRD patterns of commercial and prepared zinc oxide, mixed oxide of zinc and cobalt containing 5, 10, and 20 % cobalt, respectively, and cobalt oxide synthesized using the same methodology [26]. The 2θ angles for both commercial and prepared ZnO (31.7°, 34.4°, 36.2°, 47.5°, 56.6°, 62.9°, 66.2°, 67.9°, and 69.0°) are related to the wurtzite hexagonal structure, according to the data base used (Crystmet and PCPDFWin version 2003) and none related to the starting oxalate, confirming the oxide formation at 400 °C [29]. According to the thermal

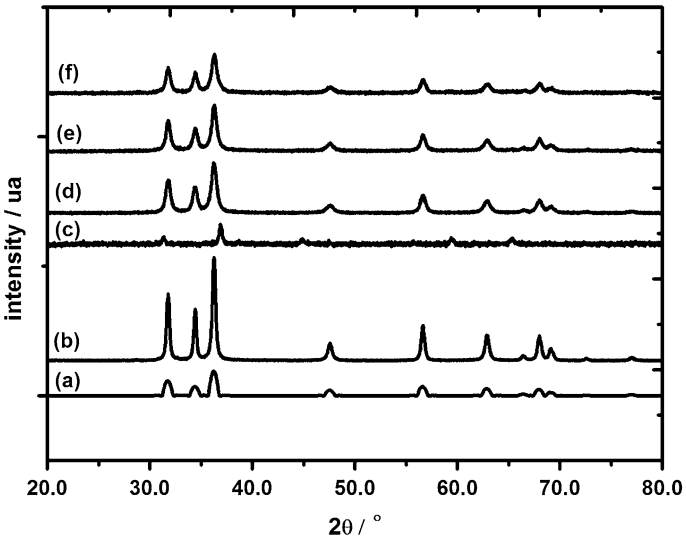

Fig. 3 X-ray diffractogram of (*a*) commercial zinc oxide; (*b*) synthesized zinc oxide; (*c*) synthesized cobalt oxide and, zinc and cobalt mixed oxides containing (*d*) 5, (*e*) 10, and (*f*) 20 % Co

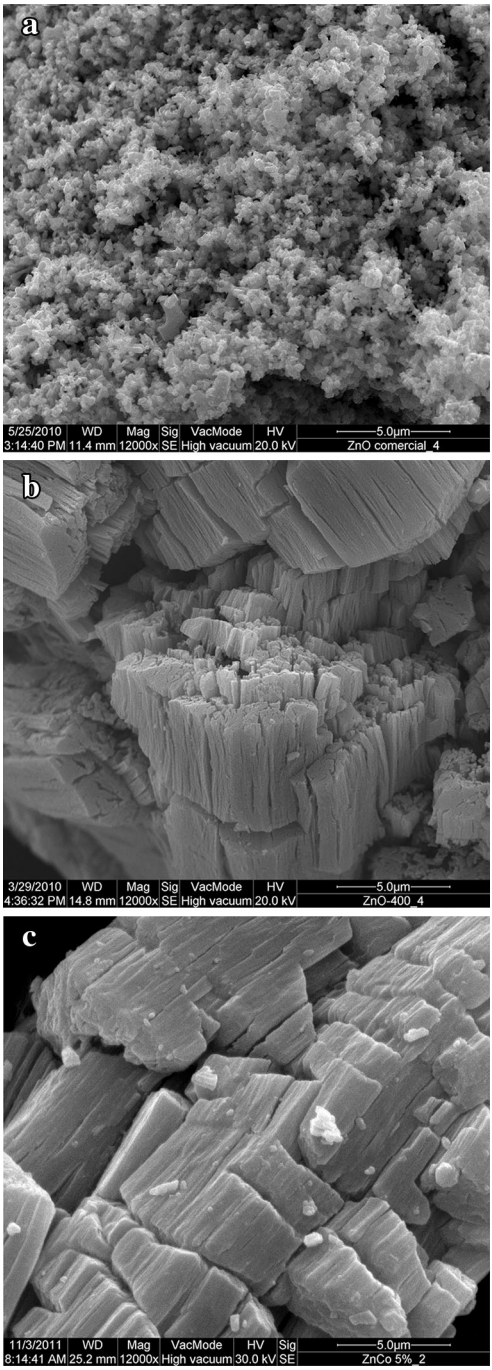

Fig. 4 SEM of **a** commercial ZnO, **b** prepared zinc oxide, and **c** zinc and cobalt mixed oxide containing 5 % Co at ×12,000 magnitude

analysis (Fig. 2) the total organic matter decomposition occurred at 400 °C, confirming its formation from the diffractograms. Beyond that, the commercial ZnO displayed lower intensity and greater enlargement in the peaks in comparison to the prepared one, indicating a lower crystallinity in the commercial sample. Meanwhile for the zinc and cobalt mixed oxide, no peak relating to cobalt oxide structure was observed, simply the decrease of the relative intensities with increase in the cobalt proportion. Thus, it is suggested that the substitution of zinc by cobalt atom had taken place, due to the approximately same ionic radii, 74 and 82 pm for zinc and cobalt, respectively. This means that there was no formation of a new phase in the mixed oxide, as well as phase segregation. The relative intensity of 2θ peak at 36.2° displayed 2087.09 counts in the oxide containing 5 % cobalt, while with 10 % Co, 1997.80 counts and, 1897.24 counts for 20 %, attributed to the zinc by cobalt replacement in the structure, decreasing the zinc diffraction intensity at the reference angle.

The images obtained from SEM of the commercial zinc oxide (Fig. 4a), prepared zinc oxide (Fig. 4b), and mixed oxide containing 5 % cobalt (Fig. 4c) with magnification of 12,000 times are shown in Fig. 4. It is observed that the prepared ZnO (Fig. 4b) presents larger and more compact particles in comparison to the commercial ZnO (Fig. 4a). This means that there was change in the oxides morphology, resulting in different behaviors during the azo dye adsorption on the surface. The mixed oxide images containing 5 % cobalt (Fig. 4c) show a similar format, but smaller than the prepared zinc oxide with cobalt oxide particles aggregated to the surface. The mixed oxides containing 10 and 20 % cobalt showed comparable morphology with respect to 5 % cobalt with increase of the particle size with increase of the dopant percentage.

The elements EDX of the investigated oxides were performed to study the composition and distribution of elements. As expected, commercial zinc oxide and the preparation showed the zinc and oxygen, while the mixed oxide containing 5 % cobalt showed zinc, oxygen, and cobalt. The distribution of these elements was uniform in these oxides. The mixed oxide containing 10 and 20 % cobalt exhibited the same characteristics in relation to 5 %, suggesting that there was not segregation phase, when the cobalt proportion was enhanced in the oxide.

The transition metal percentages in the mixed oxides were obtained quantitatively using X-ray fluorescence. It was found 4.00 % cobalt with standard deviation

Table 1 Band gap energy of commercial ZnO and zinc and cobalt mixed oxide containing different cobalt percentage and surface area calculated from BET model

% Zn	% Co	E_g (eV)	A ($m^2\ g^{-1}$)	V_{pore} ($cm^3\ g^{-1}$)	r_{pore} (nm)
100*	0	3.37	6.440	–	–
95	5	3.12	37.144	0.1119	6.026
90	10	3.22	29.785	0.1029	6.910
80	20	2.77	26.400	0.1221	6.709

* Commercial ZnO—nuclear

of 0.013 to 5 % cobalt, while the oxide containing 10 % cobalt presented 9.71 % with standard deviation of 0.019 %. Conversely, the oxide containing 20 % cobalt showed 13.98 % with standard deviation of 0.023 %. These differences could be caused by possible experimental errors, from precursors or concentration of contaminating reagents. In addition, the synthesis of mixed oxide containing 20 % cobalt could not be repeated, for lack of the same material used in all experiments for characterization and photocatalysis. Furthermore, the cobalt oxide amount on the mixed oxide surface is important in the discussion of dye adsorption capacity [30, 31]. As a function of this, it is expected that the increase of the cobalt percentage decreases the available area as well as the photocatalytic activity, taking into place that the adsorption and photocatalytic activity are directly linked [32, 33].

The energy band-gap of commercial zinc oxide and mixed oxides shown in Table 1 were obtained from the diffuse reflectance spectra using the Kubelka–Munk and Tauc methods [34, 35] displayed in Fig. 5. All the synthesized oxides showed band gap energy (E_g) lower in relation to ZnO (3.26 eV), that is, 3.12 eV to 5 % Co (Fig. 5, inset), 3.22 eV to 10 % and, 2.77 eV to 20 %. Therefore, the dopant increase in the zinc oxide structure decreases the band gap energy thereof, due to the lower band gap energy of cobalt oxide (1.4–1.8 eV) in the region of visible light [36, 37].

These results show that the synthesis was satisfactory, given that one of the objectives was to reduce the band gap energy. Conversely, this parameter is not the only one, which can justify the increase or decrease in the photocatalytic activity [31]. As previously mentioned, the photocatalytic activity of the semiconductor is related to the area available for adsorption. Among the surface areas of the oxides, calculated from the BET model, the largest surface area took place to the oxide containing 5 % cobalt (35.617 $m^2\ g^{-1}$). According to Table 1, the pore radius of the

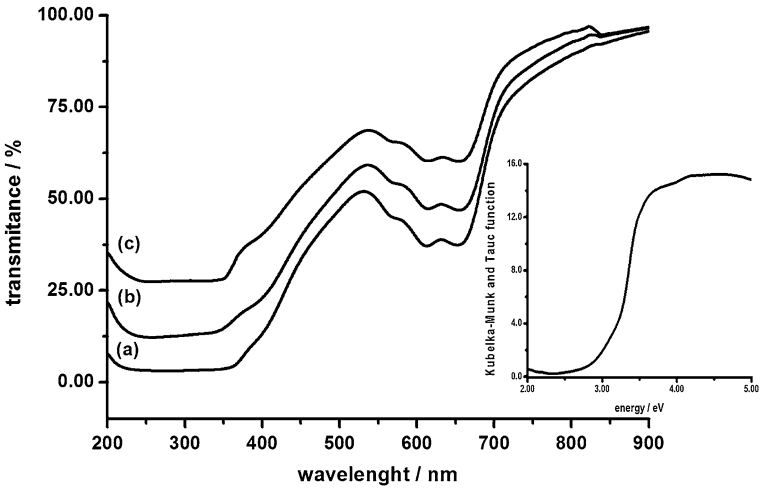

Fig. 5 UV/Vis transmittance spectra of the zinc and cobalt mixed oxides containing (*a*) 5, (*b*) 10 and, (*c*) 20 % cobalt. *Inset* Band gap energy of the mixed oxide containing 5 % cobalt evaluated by Kubelka–Munk and Tauc

oxides was around 6 nm. This means that these materials are classified as mesoporous for presenting a radius between 2 and 50 nm [38]. The DR23 adsorption on the mixed oxide surface decreased with the increase of the cobalt percentage in the dark during 60 min. The adsorption was measured by the difference between the initial and after 60 min DR23 absorptions. The commercial ZnO presented 13 % of DR23 (7.5×10^{-5} mol L^{-1}) adsorption, meanwhile the mixed oxide containing 20 % of Co was about 45 %, 10 % Co was 56 %, while for 5 % Co about 64 %. Therefore, it was attributed that the oxide with larger surface area has more available active sites that facilitate the species adsorption.

In order to verify the Direct Red 23 diazo dye (7.5×10^{-5} mol L^{-1}) decolorization, the photolysis was performed, as a control experiment, using UV irradiation during 210 min, whose decolorization efficiency was of 2 %. The photocatalytic activity of the mixed oxides and the commercial ZnO was determined under the pseudo-first order condition with a very large amount of semiconductor (0.7 g L^{-1}) containing respectively 5, 10, and 20 % cobalt in a DR23 solution (7.5×10^{-5} mol L^{-1}) at natural pH around 7.00 at 30.0 °C. The decolorization rate constants, k_{obs}, of DR23 mediated by mixed oxides as well as by commercial ZnO are presented in Table 2.

In this table, the highest k_{obs} of 14.00×10^{-3} min^{-1} occurred, following a first order behavior (r = 0.9970), when it was used the mixed oxide containing 5 % cobalt, calcined at 400 °C during 12 h. It was observed a 93 % decolorization after 150 min UV irradiation, with an intensity of 1274 mW cm^{-2}, in accordance to the initial absorbance decay at 30 °C, as shown in Fig. 6.

The mixed oxide containing 10 and 20 % cobalt displayed respectively, k_{obs} of 8.00 and 6.10×10^{-3} min^{-1} during 180 min under UV irradiation, suggesting that the proportion of increase of cobalt in the zinc oxide structure reduces the photocatalytic activity of the oxide, as observed in Table 2. Therefore, the more cobalt present on the surface, the larger the difficulty of diazo dye adsorption and decolorization. Furthermore, the rate constants are in agreement with the surface areas sizes obtained from the BET method as shown in Table 1. The mixed oxide containing 5 % cobalt displayed the highest surface area, indicating the largest available area for the dye adsorption. In addition, the pH changes during irradiation are shown in Table 2. Considering that the pK_a of ZnO is approximately 11.1 [39],

Table 2 Decolorization rate constant, k_{obs}, for DR23 (7.5×10^{-5} mol L^{-1}) in the presence of commercial ZnO and synthesized mixed oxide (0.7 g L^{-1}) and pH change as a function of irradiation time at 30 °C

% Zn	% Co	k_{obs} (10^{-3} min^{-1})	Decolorization (%)	ΔpH	*r*
100*	0	3.00	45.94	6.58–7.11 = 0.53	0.9744
95	5	14.00	93.00	6.80–6.93 = 0.13	0.9970
90	10	8.00	87.00	6.90–7.21 = 0.31	0.9673
80	20	6.10	78.00	7.17–7.65 = 0.48	0.9946

* Commercial ZnO—nuclear

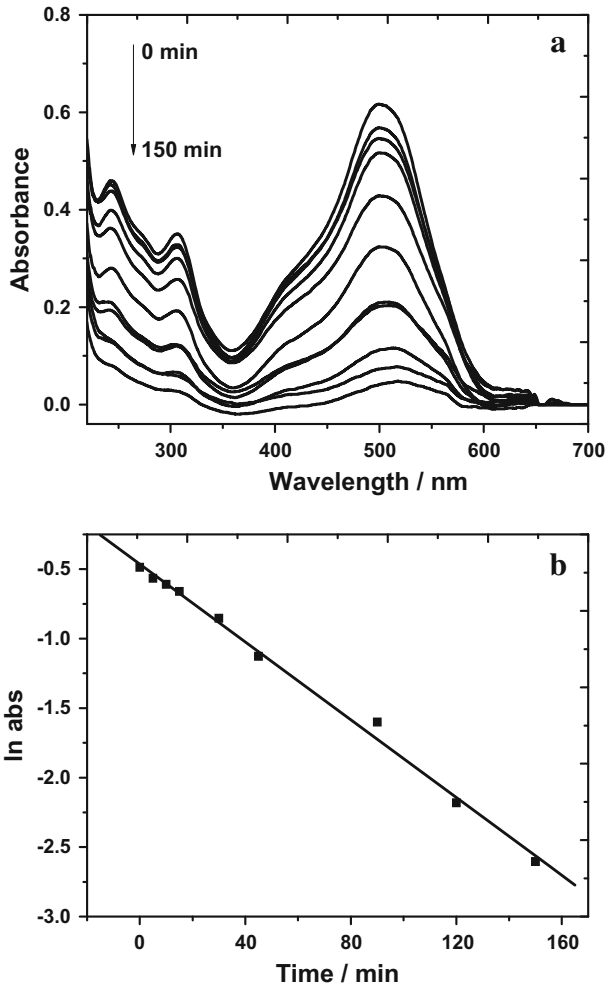

Fig. 6 **a** Decay of DR23 (7.5×10^{-5} mol L^{-1}) absorbance mediated by mixed oxide containing 5 % cobalt (0.7 g L^{-1}) as a function of the UV light irradiation time at 30 °C during 150 min. **b** Natural logarithm of (**a**) as a function of irradiation time at 30 °C

it means that the semiconductor surface in this pH range is positively charged as $ZnOH_2^+$. Thus, the approximation of a negatively charged species as sulfonate group of the diazo dye is facilitated. With respect to the commercial ZnO, the diazo dye DR23 decolorization followed the first order kinetic behavior (r = 0.9774), giving a k_{obs} of 3.00×10^{-3} min^{-1} and approximately 46 % decolorization after 210 min irradiation at 30 °C. Therefore, the decolorization rate constants of DR23 mediated by synthesized mixed oxides with respect to the commercial ZnO, were almost five-fold larger for the oxide containing 5 % cobalt, nearly tripled for 10 %, and doubled for 20 %. This may be justified by the depletion region formation in the p-n junction, which slows down the electron (e^-)/hole (h^+) pair recombination,

enhancing the hydroxyl radical generation and subsequent dye decolorization. Dong et al. observed an increase in the photocatalytic activity, attributed to the p-n junction formation, when Co_3O_4/ZnO was decolorized the methylene blue [21]. On the other hand, the ZnO, synthesized and calcined at 400 °C, decolorized 15 % during the first 8 min. The irradiation was continued for 45 min more and there was no more DR23 decolorization, indicating that the synthesized ZnO does not present the first order behavior ($r = 0.7745$). Because of this, this result was not considered for comparison with other oxides.

Conclusion

The mixed oxides were formed at 400 °C with complete oxidation of all organic matter precursors. Furthermore, the cobalt substituted the zinc in the mixed oxides and no formation of a new phase in the material was verified by XRD. All the prepared mixed oxides presented larger photocatalytic activities with respect to ZnO, due to the depletion region forming p-n junction and presented k_{obs} for DR23 decolorization larger than the commercial ZnO (3.0×10^{-3} min^{-1}) at natural pH at 30 °C. The mixed oxide containing 20 % Co was about two times faster (6.1×10^{-3} min^{-1}); for 10 % Co about three-fold (8.0×10^{-3} min^{-1}); while for 5 % about fivefold (14.0×10^{-3} min^{-1}) higher, decolorizing about 93 % diazo dye after 150 min irradiation at 30 °C.

Acknowledgments The authors thank the Fundação Araucária (22850/2011) for the financial support. Vanildo Souza Leão Neto thanks to CNPq for the IC scholarship and Thiago Orcelli thanks to CAPES by scholarship.

References

1. O'Neill C, Hawkes FR, Hawdes DL, Lourenço ND, Pinheiro HM, Delee W (1999) J Chem Technol Biotechnol 74:1009–1018
2. Herrmann JM, Vautier M, Guillard C (2001) J Catal 201:46–59
3. Legrini O, Oliveros E, Braun AM (1993) Chem Rev 93:671–698
4. Hoffmann MR, Martin ST, Choi W, Bahnemann DT (1995) Chem Rev 95:69–96
5. Gouvea AK, Wypych F, Moraes SG, Duran N, Nagata N, Zamora P (2000) Chemosphere 40:433–440. doi:10.1016/S0045-6535(99)00313-6
6. Yamazaki S, Yamabe N, Nagano S, Fukuda A (2007) J Photochem Photobiol A 185:150–155
7. Hasnat MA, Uddin MM, Samed AJF, Alam SS, Hossain S (2007) J Hazard Mater 147:471–477. doi:10.1016/j.jhazmat.2007.01.040
8. Kang SZ, Wu T, Li X, Mu J (2010) Colloids Surf A 369:268–271. doi:10.1016/j.colsurfa2010.08.029
9. Marlinda AR, Huang NM, Muhamad MR, An'amt MN, Chang BYS, Yusoff N, Harrison I, Lim HN, Chia CH, Kumar SV (2012) Mater Lett 80:9–12. doi:10.1016/j.matlet.2012.04.061
10. Shouli B, Xin L, Dianqing L, Song C, Ruixian L, Aifan C (2011) Sens Actuators B 153:110–116
11. Gnichwitz F, Marczak R, Werner F, Lang N, Jux N, Guldi DM, Peukert W, Hirsch A (2010) J Am Chem Soc 132:17910–17920
12. Israr MQ, Sadaf JR, Wilander M, Salman S, Danielsson B (2011) Appl Phys Lett 98:253705-03. doi:10.1063/1.3599583
13. Chu D, Masuda Y, Ohji T, Kato K (2010) Langmuir 26(4):2811–2815. doi:10.1021/la902866a
14. Ye FX, Ohmori A, Li CJ (2004) Surf Coat Technol 184:233–238
15. Anh BD, Kang HS, Kim JH, Kim GH, Chang HW, Lee SY (2006) J Appl Phys 100:93701

16. Atkins P, de Paula J (2006) Physical chemistry, 8th edn. Oxford, Oxford
17. Zhang Z, Shao C, Li X, Wang C, Zhang M, Liu Y (2010) Appl Mater Interfaces 2:2915–2923. doi:10.1021/am100618h
18. Wang W, Wang J, Wang Z, Wei X, Liu L, Ren Q, Gao W, Liang Y, Shi H (2014) Dalton Trans 43:6735–6743. doi:10.1039/c3dt53613k
19. Da Silva MR, De Andrade Scalvi LV, Neto VSL, Dall'Antonia LH (2015) J Mater Sci 26:7705–7714. doi:10.1007/s10854-015-3412-6
20. Zhang D (2013) Russ J Phys Chem A 87:137–144. doi:10.1134/S0036024413010068
21. Dong C, Xiao X, Chen G, Guan H, Wang Y (2015) Mater Chem Phys 155:1–8. doi:10.1016/j.matchemphys.2015.01.033
22. Kanan MW, Nocera DG (2008) Science 321:1072–1075. doi:10.1126/Science.1162018
23. McCool NS, Robinson DM, Sheats JE, Dismukes GC (2011) J Am Chem Soc 133:11446–11449. doi:10.1021/ja203877y
24. Yamada Y, Yano K, Hong DC, Fukuzumi S (2012) Phys Chem Chem Phys 14:5753–5760. doi:10.1039/c2cp00022a
25. Tang C, Wang C, Chien S (2008) Thermochim Acta 473:68–73
26. Muruganandham M, Chen IS, Wu JJ (2009) J Hazard Mater 172:706–709
27. Malecka B, Drozdz-Ciesla E (2004) Malecki A 423:13–18
28. Negi DS, Loukya B, Dileep K, Sahu R, Nagaraja KK, Kumar N, Datta R (2013) Appl Phys Lett 103:242407. doi:10.1063/1.4847775
29. Rekha K, Nirmala M, Nair MG, Anukaliani A (2010) Phys B 405:3180–3185. doi:10.1016/j.physb.2010.04.042
30. Kao CY, Liao JD, Chang CW, Wang RY (2011) Appl Surf Sci 258:1813–1818. doi:10.1016/j.apsusc.2011.10.050
31. Dodd A, McKinley A, Tsuzuki T, Saunders M (2009) Mater Chem Phys 114:382–386. doi:10.1016/j.matchemphys.2008.09.041
32. Zhang Y, Ram MK, Stefanakos EK, Goswami DY (2013) Surf Coat Technol 217:119–123. doi:10.1016/j.surfcoat.2012.12.001
33. Shimura K, Yoshida H (2012) Phys Chem Chem Phys 14:2678–2684. doi:10.1039/c2cp23220k
34. Kubelka P (1948) J Opt Soc Am 38:448–452
35. Tauc J, Grigorovici R, Vancu A (1966) Phys Stat Sol 15:627–637
36. Zheng JH, Song JL, Jiang Q, Lian JS (2012) J Mater Sci 23:1521–1526
37. Woo MA, Song MS, Kim TW, Kim IY, Ju JY, Lee YS, Kim SJ, Choy JH, Hwang SJ (2011) J Mater Chem 21:4286–4292. doi:10.1039/c0jm03430d
38. Sinhamahapatra A, Giri AK, Pal P, Pahari SK, Bajaj HC, Panda AB (2012) J Mater Chem 22:17227–17235. doi:10.1039/c2jm32998k
39. Cherginets VL, Rebrova TP (2006) Russ J Inorg Chem 51:448–487